Monotonic Response of Exposed Base Plates of Columns: Numerical Study and a New Design Method

Héctor Díaz [1], Eduardo Nuñez [2],* and Claudio Oyarzo-Vera [2]

[1] Instituto de Materiales y Modelos Estructurales, Facultad de Ingeniería, Universidad Central de Venezuela, Ciudad Universitaria, Los Chaguaramos Caracas 1051, Venezuela; hector.andres.diaz@gmail.com

[2] Depto. Ingeniería Civil. Facultad de Ingeniería, Universidad Católica de la Santísima Concepción, Alonso de Ribera 2850, Concepción 4090541, Chile; coyarzov@ucsc.cl

* Correspondence: enunez@ucsc.cl; Tel.: +56-9-5127-7382

Abstract: This paper describes a numerical study of the behavior of exposed base plates of columns under the action of axial and bending loads. The aim of this research is to evaluate numerically the failure mechanisms on stiffened and non-stiffened base plates and propose a new design method. The effects of base plate thickness, location of anchor rods, location of stiffeners and tensile strength of anchor rods were considered in the analysis. Sixteen finite elements simulations were performed considering different combinations of the above mentioned parameters. The results show a fragile response in the base plates when high resistance anchor rods are used. The anchor rods worked as fuse elements in base plates with a large thickness or many stiffeners. Additionally, the models with anchor bars located outside of the column flanges showed lower flexural strength and rotational stiffness compared to the models with anchor rods located between column flanges. The simulations showed that the base plate strength was determined by the simultaneous failure mechanisms of two or more components, different to what is stated in current design guides. Finally, the new method is suitable to design base plates with stiffened and not stiffened configurations, which unlike traditional design methods, show a good adjustment with numerical models.

Keywords: exposed column; base plate; stiffeners; yield line; anchor rods; rotational stiffness; ductility

1. Introduction

The base plates correspond to one of the most frequent column connections of steel structures. These connections are responsible for transferring loads from the superstructure to the foundations. However, the performance of these connections was deficient during recent seismic events in the USA and Japan, where significant damage and failure of these joint elements was reported [1,2].

An exposed column base consists of several components, such as: column sections, base plate, stiffeners, anchor rods, concrete foundation and shear-lug. Each of these components affects the connection's capacity to withstand axial load, shear load and bending moments. Current design methods, such as those presented in the AISC Steel Design Guide 1 [3], provide design procedures that allow for sizing of the base plate of exposed columns and their anchor rods. However, these design methods do not consider combined failure mechanisms, such as those observed in several experimental studies [4], resulting in non-conservative designs. In other cases, as the current guidelines do not consider joint configurations with stiffeners, the design often specifies plates with thicknesses that is not commercially available [5].

Numerical studies using finite elements indicate that the base plates designed using the current guidelines do not behave as expected, leading to premature crushing of concrete when using base plates

with thickness higher than 25 mm [6]. A recent experimental study on exposed base plates considering axial load and bending moment [7] showed an important correlation between the thickness of the base plate and the performance of the connection. This study concludes that despite complying with the design guidelines, flexural capacity may not be reliable due to plate interaction with other components such as the anchors. On the other hand, few studies have addressed the behavior of column bases with stiffened base plates, which are very common in the practices of detailing and construction of steel structures, as it allows for reducing the thicknesses of base plates [8,9]. However, there are no numerically or experimentally validated design procedures that consider the different performance of stiffened and non-stiffened base plates. The response of connections in terms of stiffness, strength, rotational capacity and energy dissipation is heavily dependent on the details of connection and, therefore, on the components considering their location and individual strength [10]. These problems could be alternatively solved by improving material properties or by the use of novel nanostructured materials, which have emerged to allow the synergy of high strength and high ductility modifying failure mechanisms [11]. However, it is usually preferred an engineering and constructive solution, using currently commonly used materials.

The exposed and embedded base plate connection have been researched by [12–15], obtaining that rotational fixity of base plate in steel moment resisting frames strongly influences their seismic response. However, the stiffened base plates were not considered by this investigation.

In this investigation, a numerical study on the behavior of stiffened and non-stiffened base plates is carried out, considering the contribution of different components to each configuration. The aim of the research is to evaluate numerically the failure mechanisms in stiffened and non-stiffened base plates. Additionally, due to currents design methods are focused in non-stiffened base plates a new design method is proposed. The numerical study was conducted using finite element models considering material, geometric and contact nonlinear properties. Axial load and bending moment were simultaneously applied with the goal of identifying the behavior of the base plate and its interaction with the stiffeners and anchor rods. The welds were designed to remain within the elastic range and to develop the inelastic behavior of the connected elements, being considered as ideal monolithic contacts in the numerical models. Similarly, concrete was designed to remain elastic. These conditions are like those observed on typical connection tests that intend to evaluate the seismic performance of the links, avoiding a fragile failure of elements with limited inelastic capacity, such as, welding and concrete. In the final part of the paper, the authors propose a new design method based on yield lines theory, suitable to design base plates with stiffened and not stiffened configurations.

2. Numerical Study

2.1. Specimens under Analysis

Five base plate configurations were defined by varying the location and steel quality of the anchor rods and the stiffener configuration, as shown in Figure 1. The UBP-1 configuration corresponds to a base plate model without stiffeners and anchor rods located on the outside and parallel the column flanges. The UBP-2 configuration also represents a base plate model without stiffeners, but the anchor rods are located on the outside and inside of column flanges and parallel to the section web.

The SBP-1 configuration represents a base plate model with anchor rods parallel to the flange and stiffeners between each anchor rod, while the SBP-2 configuration is similar to the previous one but without the web stiffener. Finally, SBP-3 configuration is like the SBP-1 but eliminating the web and external stiffeners. All the specimens were constructed using a standard HEB-300 columns section with ASTM-A36 steel quality [16]. All the stiffeners were 10 mm thick and made of the same material used for the column section. The specimens were modeled as cantilever elements designed to withstand axial load and bending moment.

As seen in Figure 1, each configuration has 8 anchor rods (4 on each side) with a nominal diameter of 22 mm (7/8 inch) and an embedded length of 400 mm. The analysis considered two steel qualities

for the anchor rods: ASTM-A36 quality [16] and ASTM-A193 quality [17]. The washers and the holes in the base plate were sized according to the recommendations presented in the AISC Design Guide 1 [3]. The spacing be-tween the anchor bars was selected to comply with what is specified in section D.8.2 of ACI Code 318-14 [18].

The column was supported by a square concrete foundation (700 mm × 700 mm) with a characteristic compressive strength of concrete equal to f'c = 25 MPa. The parameters considered in this analysis are presented in Table 1, where tp, g, ts, dr and Fur represents the base plate thickness, gage, stiffeners thickness, anchor rods diameter and ultimate tensile strength of anchor rods, respectively.

2.2. Finite Element Models

A numerical study was carried out using the finite element method with ANSYS software [19], considering the variables involved in the design, such as: thickness of the base plate, location of the anchor rods, stiffener configuration and ultimate tensile strength of anchor rods. Secondary components such as grouting material and leveling nuts were not included in the models.

Three dimensional models were made using SOLID 186 type finite elements to represent column, plates, anchor rods and nuts. These types of finite elements allow for the formulation of materials with plasticity, hardening, yield, large deflections and large deformations. In order to improve the computational efficiency and considering the symmetry of the models, only half of the connection was modeled, taking the mid-plane of the column web as the plane of symmetry (Figure 2).
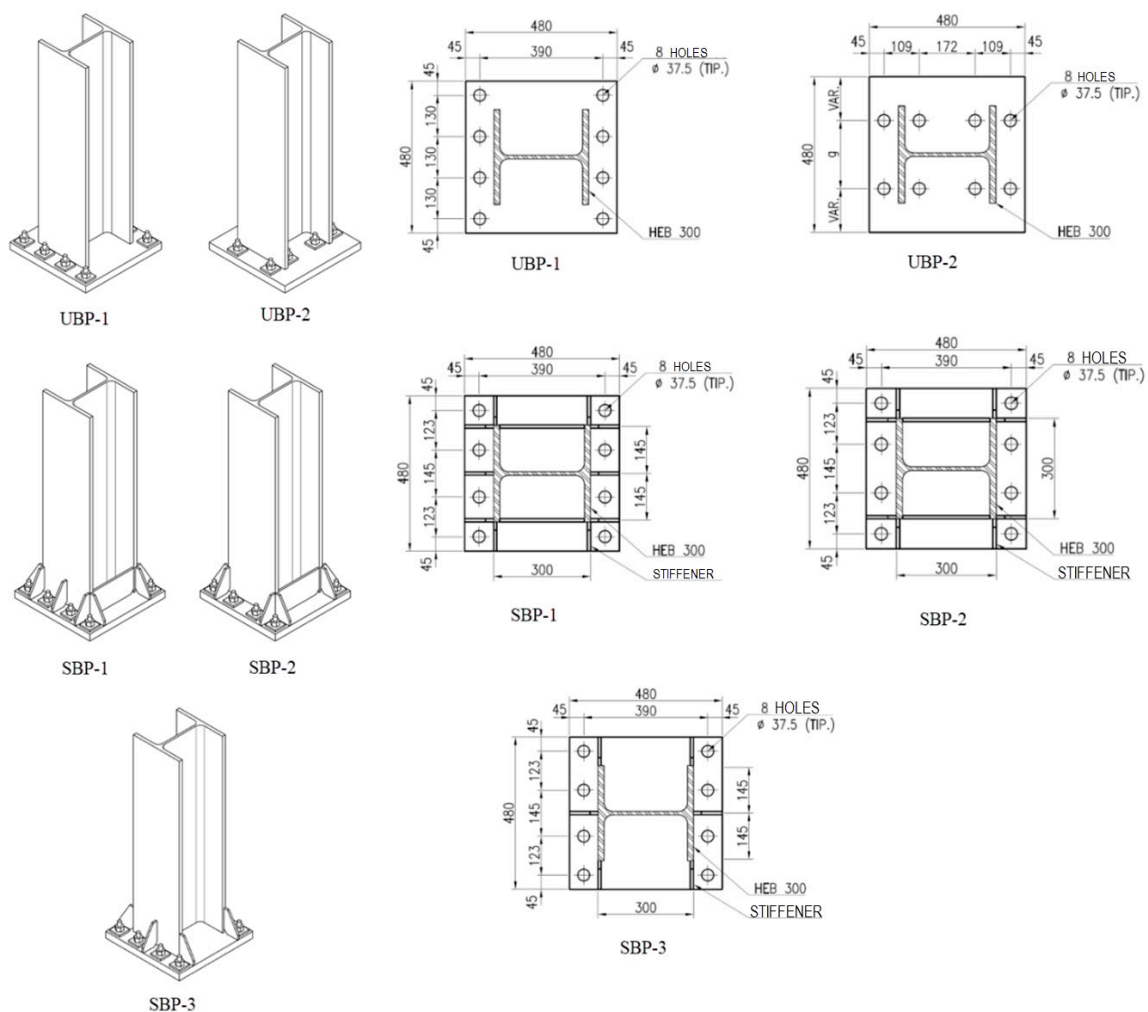
Figure 1. Specimen configurations.

Table 1. Simulations matrix.

Model	t_p (mm)	g (mm)	t_s (mm)	d_r (mm)	F_{ur} (mm)
UBP-1-1	19	N/A	N/A	22	408
UBP-1-2	25	N/A	N/A	22	408
UBP-1-3	38	N/A	N/A	22	408
UBP-1-4	19	N/A	N/A	22	878
UBP-1-5	25	N/A	N/A	22	878
UBP-1-6	38	N/A	N/A	22	878
UBP-2-1	25	210	N/A	22	408
UBP-2-2	25	390	N/A	22	408
UBP-2-3	25	210	N/A	22	878
UBP-2-4	25	390	N/A	22	878
SBP-1-1	19	N/A	10	22	408
SBP-1-2	19	N/A	10	22	878
SBP-2-1	19	N/A	10	22	408
SBP-2-2	19	N/A	10	22	878
SBP-3-1	19	N/A	10	22	408
SBP-3-2	19	N/A	10	22	878

Figure 2. Finite element models for each specimen configuration.

To incorporate the effect of diameter reducing on the anchor rods, each anchor rod on the model consists of two parts, representing the threaded section and the non-threaded section. The threaded part was modeled with an equivalent diameter, such that its cross section has the reduced area. The concrete foundation was modeled with a height equal to the embedded depth of the anchor rods (400 mm) and with fully fixed support condition in its base. Along the vertical symmetry plane, "frictionless" type constraints were assigned to simulate the behavior of the entire specimen.

Between the base plate and the surface of the foundation, a "frictional" type contact surface was assigned considering a friction coefficient between steel and concrete equal to 0.45, according to previous experimental studies [20]. Similarly, a "frictional" type contact surface was assigned between the anchor rod and the concrete with the same coefficient of friction. The nut-washer contact and anchor rod-washer contact were simulated in a simplified way by assigning "frictionless" type contacts. This type of contact allows a separation between the connected parts and a tangential movement without friction. To simulate the welded joint between the column, the base plate and the stiffeners, a "bonded" type contact was assigned, which prevents any type of relative movement.

Different constitutive laws were used to characterize the behavior of the materials considered in the model. These curves were adjusted by applying Equations (1) and (2) (actual stress and strain) to describe the multiaxial behavior of steel from the uniaxial behavior depicted by the results of the uniaxial tensile test.

$$\varepsilon_{real} = \ln(1 + \varepsilon) \tag{1}$$

$$\sigma_{real} = \sigma(1 + \varepsilon) \tag{2}$$

where,

ε = normal strain obtained from uniaxial tensile test.

σ = normal stress obtained from uniaxial tensile test.

ε_{real} = real normal strain.

σ_{real} = real normal stress.

For the ASTM-A36 steel elements (base plate, stiffeners and steel anchors), a multilinear model with hardening due to strain was used, according to [21]. The material for the high strength steel anchor rods was modeled as multilinear with hardening due to strain, according to [22]. The uniaxial compression stress–strain curve of concrete was defined as a multilinear model, according to [23,24]. The curves of the materials used are shown in Figure 3.
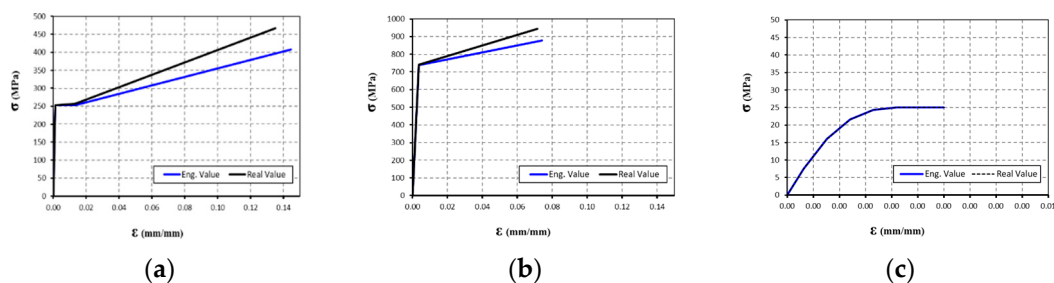
Figure 3. Constitutive models considered for (**a**) ASTM-A36 steel, (**b**) ASTM-A193 steel and (**c**) concrete.

2.3. Loading Protocol

Each specimen was analyzed under the action of a lateral load applied parallel to the column's web. Additionally, a constant compression axial load equal to 50 [T] was applied. The lateral load was applied monotonically following the scheme of a displacement protocol. These displacements were applied at 2 m above the top of the base plate, corresponding approximately to the inflection point in a column of moment resistant frame with fully fixed supports.

Under seismic conditions, a base plate can be loaded in a non-proportional manner, such that the axial load remains constant while flexural deformations vary and are reversed [4]. For this reason, the axial compression force and lateral displacement were defined in the numerical model as two separate loading steps: first the axial load is applied and then displacements are imposed until failure of the connection (Figure 4).
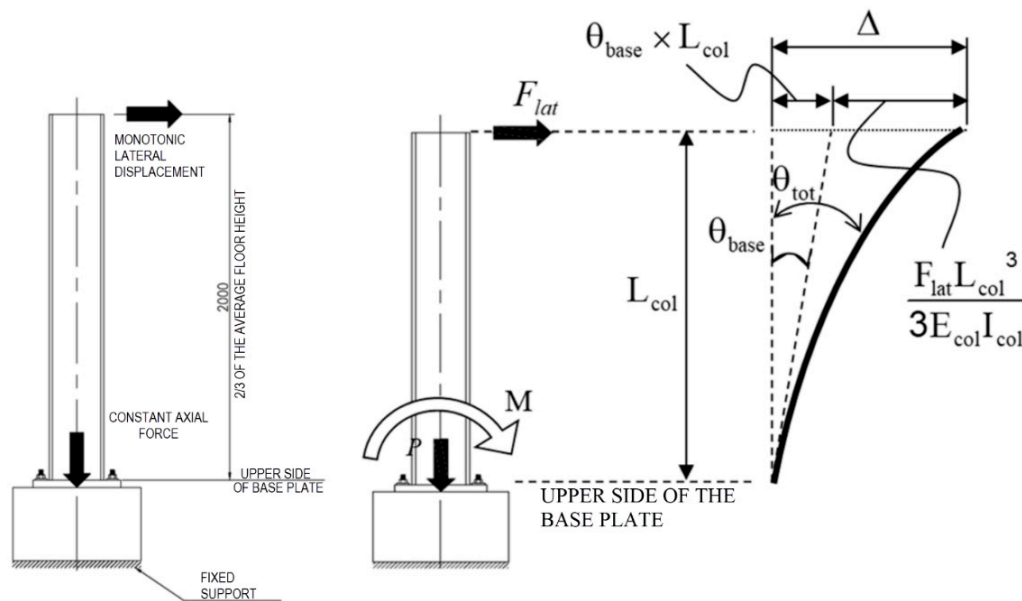
Figure 4. Loading protocol and response parameters.

2.4. Response Parameters

In each of the simulations, the lateral force was recorded according to the displacement protocol applied at the top of the column, as well as the sliding measured at the bottom of the base plate. From these results, the moment–rotation response was obtained using the following equations:

$$M = F_{lat} \times L_{col} \tag{3}$$

$$\theta_{base} = \left(\Delta - \frac{F_{lat} \cdot L_{col}^3}{3 \cdot E_{col} \cdot I_{col}} \right) \cdot \frac{1}{L_{col}} \tag{4}$$

where,

F_{lat} = Lateral load.
Δ = Relative displacement between top and base of the column.
E_{col} = Column Young's modulus (2.1×10^5 MPa).
I_{col} = Moment of inertia of the column section.
L_{col} = Load application point height.

From the moment–rotation curves the following results were obtained (Figure 4): Maximum connection moment, (Mmax), yielding moment of the connection (My), rotation at yielding (θy), rotation at maximum moment (θ_max) and the elastic rotational stiffness of the connection ($\beta y = My/\theta y$).

3. Model Results

3.1. Influence of the Base Plate Thickness

As shown in Figure 5a, three failure mechanisms were obtained in which inelastic incursion of two or more components simultaneously occurs in the tensile and compression zones. The first failure mechanism consisted of a fracture of the anchor rods in the tensile zone and concrete crushing in the compression zone. This failure mode is representative of the response observed in simulations UBP-1-3 and UBP-1-6. Moderate yielding was observed in the base plate. A second failure mechanism occurs due to the formation of a plastic joint line in the compression zone of the base plate, accompanied by the tensile fracture of the anchor bars. This fault mechanism was observed in the UBP-1-2 simulation.

The third mode of failure occurs due to the initial formation of a plastic joint line at each end of the base plate, which are subsequently accompanied by the fracture of the anchor bars. In this case, high levels of inelastic deformation are observed in the base plate (0.13 mm/mm), which indicates that the base plate has reached its fracture tension. This behavior is observed in the simulations corresponding to models UBP-1-1, UBP-1-4 and UBP-1-5 (see Figure 5b).
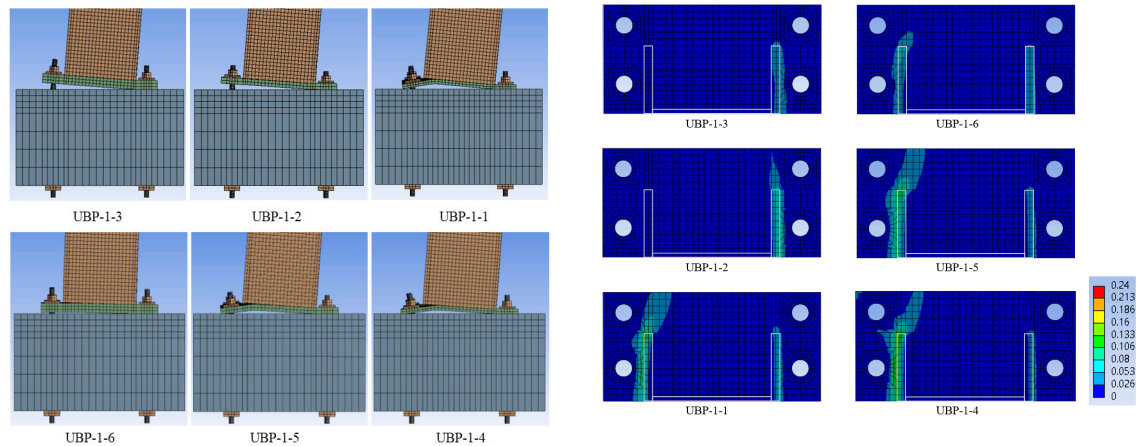
(**a**) Deformation at base plate.

(**b**) Plastic strain distribution (mm/mm).
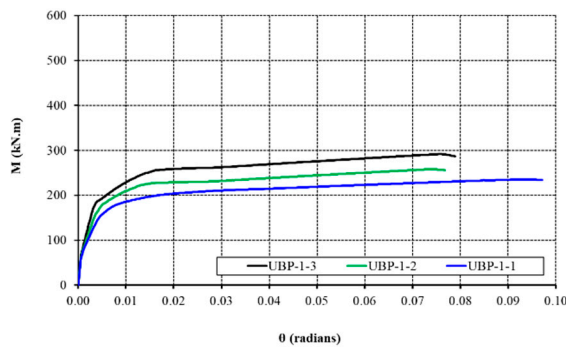
(**c**) Moment–rotation curves models UBP-1-1, UBP-1-2 and UBP-1-3.
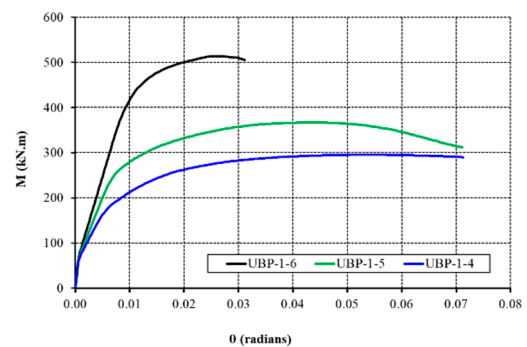
(**d**) Moment–rotation curves models UBP-1-4, UBP-1-5 and UBP-1-6.
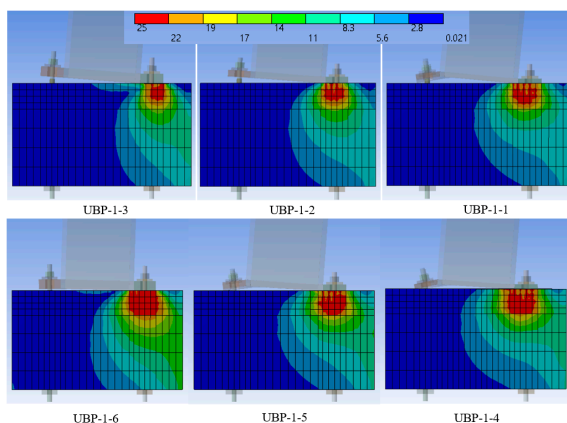
(**e**) Von-Mises stress distribution in concrete (MPa).

Figure 5. Influence of base-plate thickness model UBP-1.

In Figure 5c, a larger strength and greater elastic stiffness can be observed in the UBP-1-3 model and a deformability and inelastic behavior like the UBP-1-2 model. This is because in both models the

inelastic deformations are mainly concentrated in the anchor rods, which have a great deformability. An increment in the resistant moment was observed by increasing the thickness of the base plate by 13% between the UBP-1-2 and UBP-1-3 models and increase of 9.5% between the UBP-1-1 and UBP-1-2 models. In the case of models whose fault is governed by the fracture of ASTM-A36 anchor rods, a high rotational capacity was observed (approximately 0.075 rad).

As can be seen in Figure 5d, the initial stiffness and strength of the connection increase with the thickness of the base plate and ductility reduction. These results show that the column bases with thinner base plates are characterized by low resistance and initial stiffness, accompanied by a more ductile behavior, reaching rotations of up to 0.095 rad, in which inelastic deformations are mainly concentrated in the base plate. These types of connections are the most suitable to an "articulated" condition when they incur within the inelastic range. When observing the moment–rotation response of the UBP-1-6 model, a rotation capacity of θmax = 0.026 rad is obtained, being 67% smaller than the UBP-1-5 model and 107% smaller than the UBP-1-4 model. However, this model has an average resistance 54% higher than the other two models.

The tension distribution in the concrete due to the pressure applied by the base plate is shown in Figure 5e. A variation of the area in which the maximum tensions are concentrated was observed, which was dependent on the thickness of the base plate. In general, it can be seen that in the case of models with more rigid base plates (38 mm), the maximum tensions are concentrated at the end of the base plate, unlike the models with more flexible base plates (19 mm) where the stresses are distributed over a wider area once the flexural yielding of the base plate occurred.

In summary, in the non-stiffened base plates with A36 steel anchor rods, a loss of ductility appears as the thickness increases and the inelastic incursion is concentrated in anchor rods. Therefore, when A193 steel anchor rods are used, a loss of ductility with increase of strength and stiffened is reached as the thickness of the base plate increases. These effects must be considered in the global seismic analysis of steel structure.

3.2. Influence of the Anchor Rods Configuration

The specimens UBP-1-2, UBP-2-1 and UBP-2-2 (25 mm thick base plates, without stiffeners) were fixed to the base by ASTM A36 anchors rods, and in UBP-1-5 models, the specimens UBP-2-3, UBP-2-4 (25 mm thick base plates, without stiffeners) were fixed with ASTM A193 anchors anchor rods. These two kinds of configurations were compared in order to assess the effect of the anchor strength on the yielding pattern and failure mode of the connection.

As can be seen in Figure 6a, the location of the anchor bars significantly affected the distribution of base plate's deformations, being more evident in the tensile zone of the models with high strength anchor bars. Additionally, a lower plastic deformation was observed in the base plates where anchor bars are located parallel and closer to the column web (UBP-2-1 and UBP-2-3). This condition suggests the base plates have a larger bending strength when fixed following this anchor setting.

In the configurations with ASTM A36 steel anchor rods, a similarity was observed in the resistant moment of the column bases with anchors parallel to the column web (UBP-2-1 and UBP-2-2), as shown in Figure 6b. The difference between the resistant moment of these two connections was 1.2%. In both cases the fault was governed mainly by the fracture of the anchor rods, and not by the flexural yielding of the base plate in the traction zone. On the other hand, there was also a lower strength in the column base with anchor bars parallel to the flanges (UBP-1-2), due to the difference between the lever arms, reaching rotations larger than 0.07 rad.

In the configurations with ASTM A193 anchor bars, a concentration of the plastic deformations in the base plate or the anchor bars is evidenced depending on their configuration. As can be seen in Figure 6b,c, the UBP-2-3 model had a significantly higher strength, giving a moment 35% larger than the UBP-2-4 model. This demonstrates that the flexural strength of the base plate in the tensile zone was influenced by the distance of the anchor rods to the web of the column, which in turn has an influence on the resistant moment of the connection.
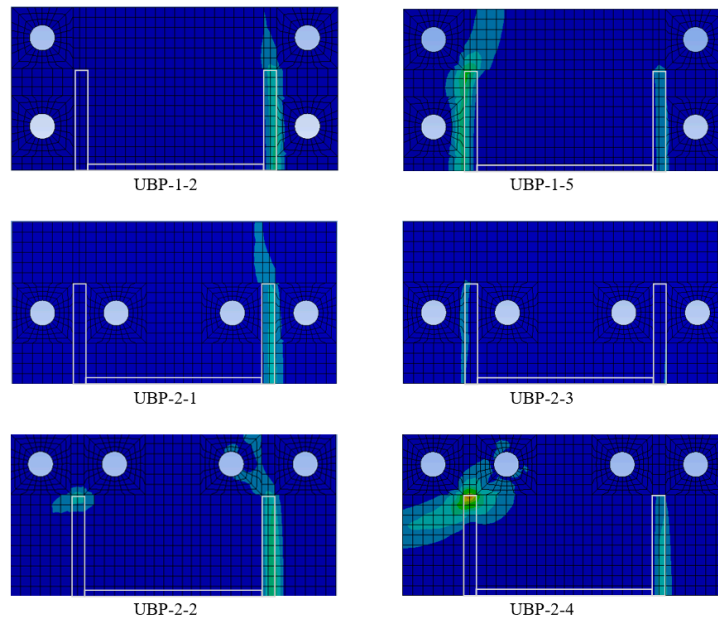
(**a**) Plastic strain distribution (mm/mm).
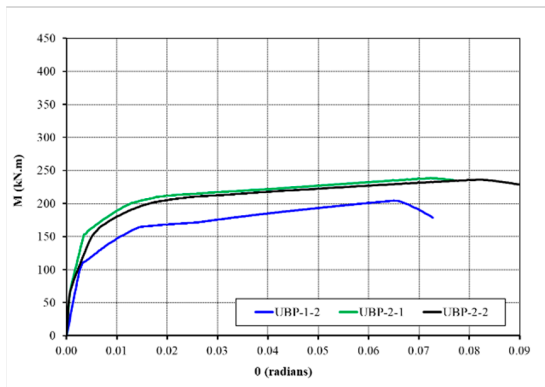
(**b**) Moment–rotation curves models UBP-1-2, UBP-2-1 and UBP-2-2.
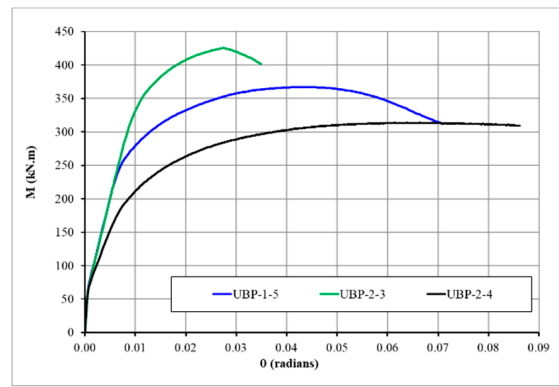
(**c**) Moment–rotation curves models UBP-1-5, UBP-2-3 and UBP-2-4.

Figure 6. Influence of the anchor rods configuration.

In Figure 6b,c, a lower elastic rotational stiffness and a lager ductility can be seen in those column bases whose anchor bars were located away from the column web and outside of the column flanges (UBP-2-2 and UBP-2-4). This indicates that the location of the anchor groups did not significantly influence the stiffness, but it is important to determine flexural deformation of the base plate in the traction zone.

In summary, a minor ductility was obtained in the non-stiffened base plates with A36 steel anchor rods, as the anchor rods configuration was similar to end-plate configuration. However, an inclined failure mechanism was obtained with anchor rods near from weak axis column restricting the flexural capacity of base plate. Therefore, when A193 steel anchor rods were used a loss of ductility with increase of strength and stiffness was reached, as the anchor rods were located according to end-plate configuration. These effects must be considered in the global seismic analysis of steel structure.

3.3. Influence of the Stiffener Configuration

The effect of the stiffener configuration on the behavior of the exposed stiffened column bases was characterized from three base plate configurations, SBP-1, SBP-2 and SBP-3. Each of these

configurations was studied with standard steel anchor rods and high strength anchor rods in order to provide a better understanding of the effect this parameter had on the yield pattern and the mode of failure of the column bases with stiffened base plates.

Figure 7a shows that the greater the amount and location of the stiffeners, the more significant the changes in the failure mechanism experienced by the connection. These changes were more relevant in the tensile zone of the models with high strength anchor bars, in which yield was mainly concentrated in the base plate, reaching high levels of plastic deformation (0.10 mm/mm).
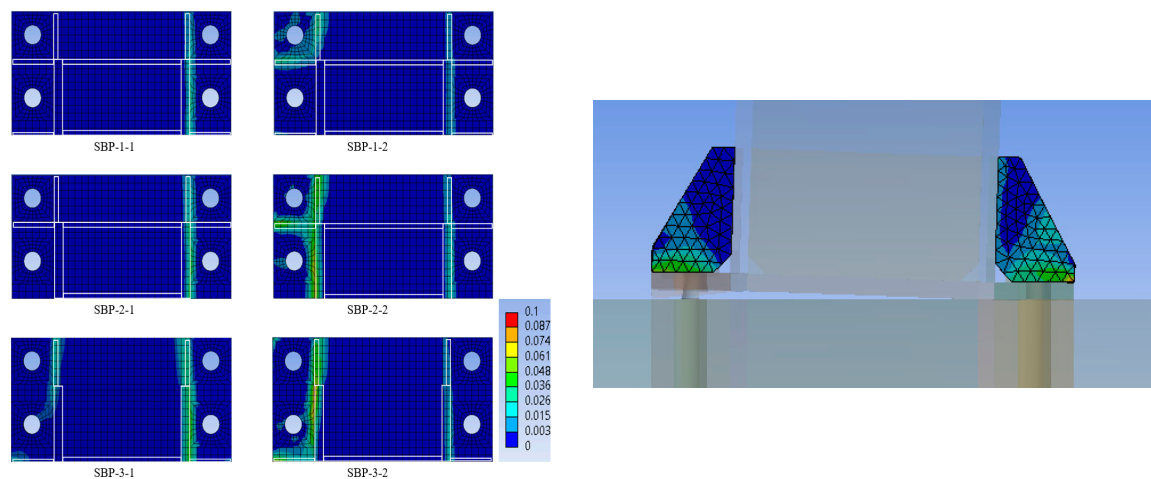
(**a**) Plastic strain distribution (mm/mm).

(**b**) Plastic strain distribution on stiffeners (mm/mm).
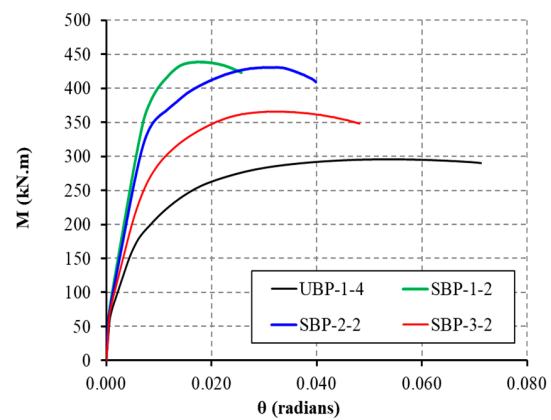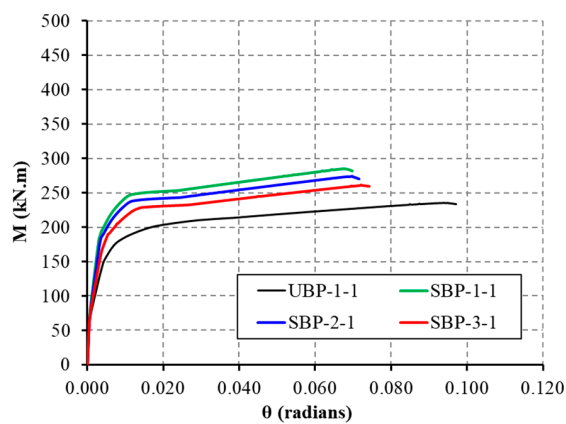
Figure 7. Influence of the stiffener configuration.

As for the yield pattern presented on the base plate of SBP-1-2 model, a concentration of the plastic deformations was observed in the corner, while other areas remained elastic. This is explained by the less favorable stiffening conditions of the corners that had two continuous edges and two free edges, while the central panels had three continuous edges and only one free edge. In the tensile zone of the base plate of models SBP-2-2 and SBP-3-2, a more uniform distribution of yield was observed. Additionally, in all of the models, flexural yield was reached in the compression zone of the base plate and axial yield (tension or compression) on the stiffener (see Figure 7b).

The moment–rotation curves presented in Figure 7c,d show small differences in the resistant moment of the group of column bases with stiffeners. On average, the resistant moment of these three connections differed only by 4.5%. This difference, although not very significant, could mainly be attributed to the resistance provided by the stiffeners in the compression zone, where the amount varies for each model. On the other hand, these specimens show a good rotation capacity, reaching rotations

close to 0.07 rad. This relatively high ductility was provided by the deformation capacity of the anchor rods, which in this case were made of ordinary steel (ASTM A36).

In the column bases with high strength anchor bars (ASTM A193) a different behavior was observed. Inelastic deformations were concentrated in the base plate or the anchor rods depending on the amount and configuration of the stiffeners. The moment–rotation curves of Figure 7 show that connections SBP-1-2 and SBP-2-2 models had similar moment resistance (only a 1.7% of difference), although they had different amounts of stiffeners. The same figure also shows that SBP-2-2 model reached a maximum rotation of 87% greater than that achieved by the SBP-1-2 model, showing that the amount and configuration of stiffeners affected the strength and ductility of exposed column bases. On the other hand, when comparing the response of the SBP-2-2 and SBP-3-2 models, a moderate increase in the resistant moment and the rotational stiffness (18% in both cases) was observed, while the rotational capacity (θmax) did not vary significantly (6% difference). As mentioned in before cases with variable thickness and anchor rods location, a minor ductility was obtained in stiffened base plates when A36 steel anchor rods were used. Therefore, an increase in number of stiffeners conducted to greater levels to flexural resistance and a loss of ductility. These effects must be considered in the global seismic analysis of steel structure.

4. Design Methods

4.1. Current Methods for the Assessment of the Bending Strength of Non-Stiffened Base Plates

Currently, the flexural strength of base plates was evaluated by 3 methods: two of them, described in [3], are based on the characterization of concrete stresses on the base plate; while the third, described in [25], corresponds to a component method.

The first method presented in [3] is known as the triangular stress block (TSB) method. This method assumes a triangular distribution of the stresses in the concrete, being the bending strength obtained from the quantification of 3 resistance limit states: (i) tensile rupture of the anchor bars, (ii) flexural yielding of the base plate at the compression interface and (iii) flexural yielding of the base plate at the tension interface.

The second method presented in [3] is known as the rectangular stress block (RSB) method, and it assumes a rectangular distribution of the stresses in concrete, which is the bending strength obtained from the quantification of the same resistance limit considered for the TSB method. In both methods and for all the considered cases, the bending strength is controlled by the flexural yielding of the base plate at the compression interface.

These methods are not applicable to non-stiffened base plates with two rows of bolts per flange (such as type UBP-2) and neither to stiffened base plate configurations, because the methods do not consider the stiffeners contribution to the strength of connections. The finite element model (FEM) results presented in Figures 8 and 9 show a bending capacity of the connection larger than the estimation calculated by applying the TSB and RSB methods, being significantly more conservative design methods in the case of base plates without stiffeners with one row of anchors.

The third method, the component method (CM) [25], quantifies the bending strength of the connection from the strength capacity of each element that forms the connection. In all the cases considered by this method, the bending strength is controlled by the flexural yielding of the base plate at the tension interface, except for the cases UBP-2-3 and UBP-2-4, where strength is controlled by the flexural yielding of the base plate at the compression interface.

Similar to the TSB and RSB methods, the CM method is not applicable to both non-stiffened base plates with two rows of bolts per flange (such as type UBP-2) and stiffened base plate configurations, because the methods do not consider the stiffeners' contribution to the strength of connections. Figure 10 shows a bending capacity of the connection larger than the estimation calculated by applying the CM method, being more in the case of connection UBP-2-3 and UBP-2-4.
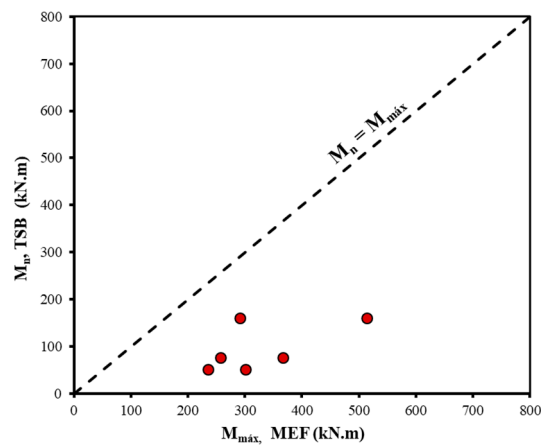
Figure 8. Comparison of FEM results with estimations of the triangular stress block (TSB) method.
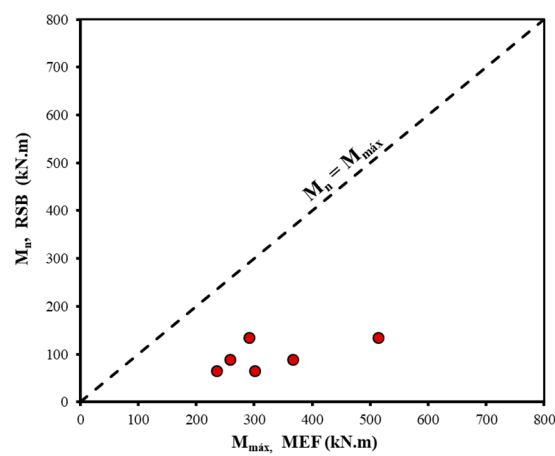
Figure 9. Comparison of FEM results with estimations of the rectangular stress block (RSB) method.
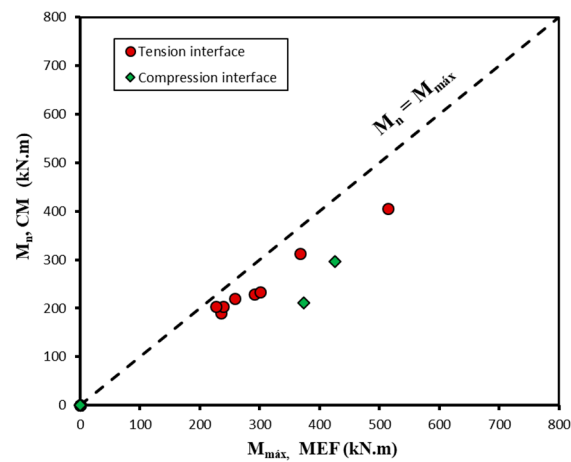
Figure 10. Comparison of FEM results with estimations of the component method (CM).

4.2. Proposed Methods for the Assessment of the Bending Strength of Stiffened and Non-Stiffened Connections

The behavior observed in finite element simulations suggests that the maximum strength of the connection was controlled by different limit states associated to different collapse mechanisms. In this sense, the current design methods did not allow for accurately reproducing the flexural strength, often resulting conservative designs and excluding stiffener base plates configurations that are frequent and necessary in professional practice.

The novel method proposed here considered the following limit states: (i) flexural yielding of the base plate, both in the tension zone and in the compression zone (LS1); (ii) flexural yielding of the base plate and ultimate failure of the anchor bars in the tension interface, combined with flexural yielding of the base plate at the compression interface (LS2); (iii) ultimate failure of the anchor bars at the tension interface and flexural yielding of the base plate at the compression interface (LS3); (iv) ultimate failure of the anchor bars in the tension interface and bearing of concrete in the compression interface (LS4) and (v) flexural yielding of the base plate and ultimate failure of the anchor bars in the tension interface, combined with concrete bearing in the compression interface (LS5).

In this novel method, the flexural strength was obtained from the application of the yielding lines theory, by applying a balance between the work of the external forces and the work of the internal forces that occurs for the different collapse mechanisms. Tables 2–6 show the collapse mechanisms that control the flexural strength of the base plates UBP-1, UBP-2, SBP-1, SBP-2 and SBP-3, respectively. These tables show the parameterized flexural strength for each failure mechanism.

The flexural strength calculated from non-stiffened base plates by applying the proposed method are compared with the results of FE model results are presented in Figure 11. An acceptable level of coincidence was observed with differences smaller than 5% for non-stiffened base plates, obtaining a better prediction than the one obtained by applying TSB, RSB and EC3. In the case of stiffened base plates, the flexural strength obtained by applying the proposed method achieved an acceptable match with the results of FE simulations, with differences smaller than 5%, as shown in Figure 12. This kind of stiffened base plate configuration is not considered by traditional methods.
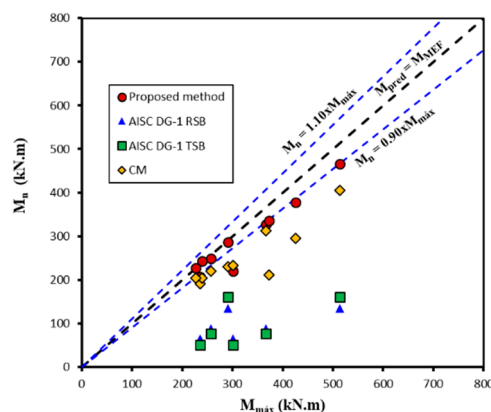
Figure 11. Comparison of flexural strength estimations of the different methods with FEM results for non-stiffened base plates.
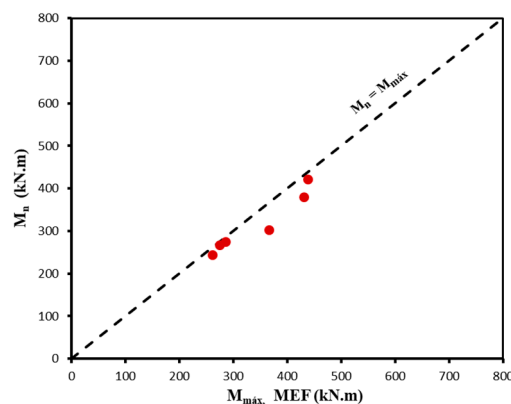
Figure 12. Comparison of flexural strength estimations of the proposed method with FE models results for stiffened base plates.

Table 2. Limit states that control the design of base plate type UBP-1.

LS1

$$M_p^1 = M = 2m_p B\left(1 + \frac{d}{pf_o}\right) + P\left(\frac{d}{2}\right)$$

LS2

$$M_p^2 = M = m_p B\left(2 + \frac{d}{d_e + pf_o}\right) + n_r T_r d_e\left(\frac{d}{d_e + pf_o}\right) + P\left(\frac{d}{2}\right)$$

LS3

$$M_p^3 = M = m_p B + n_r T_r d_e(d + pf_o) + P\left(\frac{d}{2}\right)$$

LS4

$$M_p^4 = M = n_r T_r(N - Y - d_e) + \frac{BY^2}{2}f_{p(\max)} + P\left(\frac{N}{2} - Y\right)$$

LS5

$$M_p^5 = M = m_p B\left(\frac{N - Y}{d_e + pf_o}\right) + n_r T_r\left(\frac{N - Y}{d_e + pf_o} - 1\right)d_e + \frac{BY^2}{2}f_{p(\max)} + P\left(\frac{N}{2} - Y\right)$$

Table 3. Limit states that control the design of base plate type UBP-2.

LS1

$$M_p^1 = m_p \left\{ 2B \left[h_i \left(\frac{1}{s} + \frac{1}{pf_i} \right) + h_o \left(\frac{1}{pf_o} \right) \right] + \frac{8}{g} h_i (pf_i + s) \right\} + P \left(\frac{d}{2} \right)$$

LS2

$$M_p^2 = M = m_p B \left(2 + \frac{d}{d_e + pf_o} \right) + 2T_r d_e \left(\frac{h_i}{d_e} + \frac{d}{d_e + pf_o} \right) + P \left(\frac{d}{2} \right)$$

LS3

$$M_p^3 = M = m_p B + 2T_r (h_i + h_o) + P \left(\frac{d}{2} \right)$$

LS4

$$M_p^4 = M = 2T_r (h_i + h_o - 2Y) + \frac{BY^2}{2} f_{p(\max)} + P \left(\frac{N}{2} - Y \right)$$

LS5

$$M_p^5 = M = m_p B \left(\frac{N - Y}{d_e + pf_o} \right) + 2d_e T_r \left(\frac{h_i - Y}{d_e} + \frac{N - Y}{d_e + pf_o} - 1 \right) + \frac{BY^2}{2} f_{p(\max)} + P \left(\frac{N}{2} - Y \right)$$

Table 4. Limit states that control the design of base plate type SBP-1.

LS1

$$M_p^1 = m_p\left\{2Bh_o\left(\frac{1}{pf_o} + \frac{1}{2s}\right) + 8\left[\frac{D(g'-D) + g(D-g)}{g(D-g)(g'-D)}\right]h_o(pf_o + d_e)\right\} + m_{p,eq}B + P\left(\frac{d}{2}\right)$$

LS2

$$M_p^2 = 2m_p\left[\left(\frac{B-D}{2}\right)\left(1 + \frac{d}{a}\right) + (d+a)\left(\frac{a+pf_o+d_e}{b} + \frac{b}{a}\right)\right] + m_{p,eq}B +$$
$$2T_r\left[pf_o + d\left(2 - \frac{pf_o}{a}\right)\right] + P\left(\frac{d}{2}\right)$$

LS3	Idem to UBP-1
LS4	Idem to UBP-1

LS5

$$M_p^5 = 2m_p\left\{\frac{(B-D)}{2}\left[1 + \frac{h_o - Y - pf_o}{a}\right] + (h_o - Y - pf_o + a)\left(\frac{a+pf_o+d_e}{b} + \frac{b}{a}\right)\right\} +$$
$$2T_r\left[pf_o + (h_o - Y - pf_o)\left(2 - \frac{pf_o}{a}\right)\right] + \frac{BY^2}{2}f_{p(max)} + P\left(\frac{N}{2} - Y\right)$$

Table 5. Limit states that control the design of base plate type SBP-2.
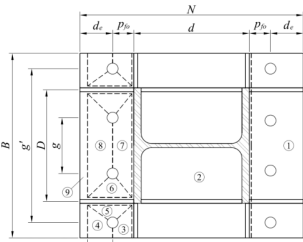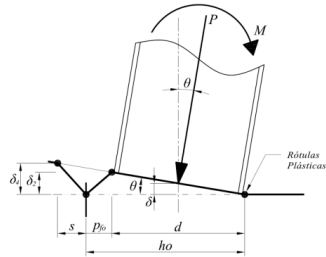
LS1	 $$M_p^1 = m_p\left\{2Bh_o\left(\frac{1}{pf_o} + \frac{1}{s}\right) + 8\left(\frac{1}{D-g} + \frac{1}{g'-D}\right)h_o(pf_o + s)\right\} + m_{p,eq}B + P\left(\frac{d}{2}\right)$$
LS2	Idem to SBP-1
LS3	Idem to SBP-1
LS4	Idem to SBP-1
LS5	Idem to SBP-1

Table 6. Limit states that control the design of base plate type SBP-3.
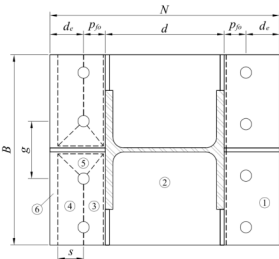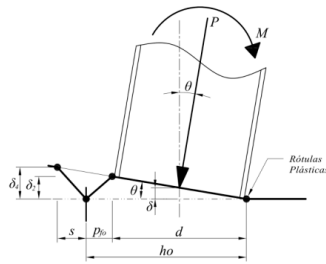
LS1	$$M_p^1 = m_p\left[2Bh_o\left(\frac{1}{pf_o} + \frac{1}{s}\right) + \frac{8}{g}h_o(pf_o + s)\right] + m_{p,eq}B + P\frac{d}{2}$$
LS2	$$M_p^2 = 2m_p\left[\frac{B}{2}\left(1 + \frac{d}{a}\right) + (d+a)\left(\frac{2a}{b} + \frac{b}{a}\right)\right] + m_{p,eq}B + 4T_r(d+a) + P\frac{d}{2}$$
LS3	Idem to SBP-1
LS4	Idem to SBP-1
LS5	$$M_p^5 = 2m_p\left[\frac{B}{2}\left(\frac{N-Y}{a}\right) + (N-Y)\left(\frac{2a}{b} + \frac{b}{a}\right)\right] + 4T_r\left(\frac{N-Y}{a} - 1\right)d_e + \frac{BY^2}{2}f_{p(max)} + P\left(\frac{N}{2} - Y\right)$$
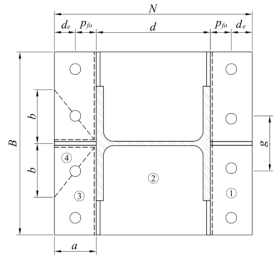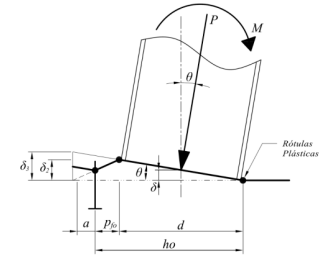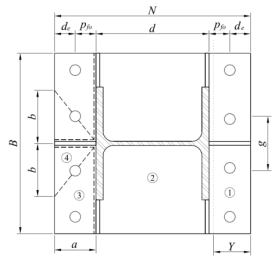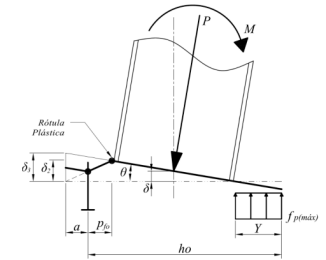
5. Conclusions

In this study, the response of 16 configurations of stiffened and non-stiffened base plates was evaluated using FE models. The behavior of a column's exposed base plates considering the influence of the base plate thickness, location of anchor rods and stiffener configuration, subjected to axial load and moment was evaluated, and a new design method was proposed. The conclusions are shown as follows:

From the results of the numerical simulations, thick base plates presented greater strength and elastic stiffness compared to thin base plates with a less ductile behavior. In these cases, the failure mechanism was controlled by a fracture of anchor rods in the tension zone and concrete bearing in the compression zone. The ductility loss was more significant in cases when the connection resistance was conditioned by the tensile fracture of high strength anchor bars. In those cases, in which regular strength steel anchor bars were used, the influence of base plate thickness on the rotation capacity was not significant, because inelastic deformations were mainly concentrated on anchor rods, which had a larger deformation capacity compared to high strength anchor bars.

The base plate configurations with anchor rods located between the column flanges required a smaller thickness. However, when high strength anchor rods were used, this configuration showed a less ductile behavior. Base plate configurations with anchor rods parallel to the column web and outside of the column flanges reported the lowest flexural strength and elastic rotational stiffness. This typology required thicker base plates and larger anchor rods diameter. However, this configuration was more ductile, especially in cases where high strength anchor rods were used.

A significant increase in flexural strength and rotational stiffness was obtained when stiffeners were included in base plate configuration, but there was also a considerable decrease in ductility. This was more significant when the failure was conditioned by fracture of high strength anchor rods. In the case of stiffened base plate connections with regular strength anchor rods, no significant change in strength and stiffness was observed when the stiffeners quantity was varied. The results obtained from the models with high strength anchor rods revealed that an excessive number of stiffeners was associated with a loss of ductility, without a significant contribution to the resistance and rotational stiffness.

The proposed method allowed an acceptable adjustment with FE models unlike the traditional design methods with differences smaller than 5%. Additionally, an identification of failure mechanisms for stiffened and non-stiffened base plates was obtained. Unlike analytical methods, the FE models verified that the maximum resistance of a base plate was conditioned by the simultaneous occurrence of the different failure mechanisms and not by the individual failure of any of its components. In addition, contrasting with the traditional methods, the new design method can estimate the flexural strength of stiffened and non-stiffened base plates, conducting to lighting solutions for base plates.

Author Contributions: Conceptualization, E.N.; Methodology, E.N.; Investigation, H.D. and E.N.; Writing—original draft, E.N. and C.O.-V.; Writing—review and editing, E.N. and C.O.-V.; Funding acquisition, E.N.; Resources, E.N.; Supervision, E.N. and C.O.-V. All authors have read and agreed to the published version of the manuscript.

Funding: This research received no external funding.

Conflicts of Interest: The authors declare no conflict of interest.

References

1. Grauvilardell, J.; Lee, D.; Hajjar, J.; Dexter, R. *Synthesis of Design, Testing and Analysis Research on Steel Column Base Plate Connections in High-Seismic Zones*; Structural Engineering Report, No. ST-04-02. Technical Report; Department of Civil Engineering, University of Minnesota: Minneapolis, MN, USA, October 2005.
2. Fahmy, M. Seismic Behavior of Moment-resisting Steel Column Bases. Ph.D. Thesis, Department of Civil and Environmental Engineering, University of Michigan, Ann Arbor, MI, USA, 2000.
3. Fisher, J.M.; Kloiber, L.A. *Steel Design Guide Series 1–Base Plate and Anchor Rod Design*, 2nd ed.; American Institute of Steel Construction: Chicago, IL, USA, 2006.

4.   Gomez, I.; Kanvinde, A.; Smith, C.; Deierlein, G. *Exposed Column Base Connections Subjected to Axial Compression and Flexure*; Technical Report; American Institute of Steel Construction, AISC: Chicago, IL, USA, August 2010.

5.   Kanvinde, A.; Jordan, S.; Cooke, R. Exposed column base plate connections in moment frames—Simulations and behavioral insights. *J. Constr. Steel Res.* **2013**, *84*, 82–93. [CrossRef]

6.   Lee, D.; Goel, S.; Stojadinovic, B. Exposed column-base plate connections bending about weak axis: I. Numerical parametric study. *Int. J. Steel Struct.* **2008**, *8*, 11–27.

7.   Lim, W.; Lee, D.; You, Y. Exposed column-base plate strong-axis connections for small-size steel construction. *J. Constr. Steel Res.* **2017**, *137*, 286–296. [CrossRef]

8.   Blodgett, O. *Design of Welded Structures*; The James F. Lincoln Arc Welding Foundation: Cleveland, OH, USA, 1966; Volume 3.3, pp. 1–32.

9.   Karbakhsh, A.; Bin, I.; Binti, Z. Finite element analysis of bolted column base connection without and with stiffeners. *Int. J. Phys. Sci.* **2011**, *6*, 1–7.

10.   Latour, M.; Rizzano, G. Mechanical modelling of exposed column base plate joints under cyclic loads. *Eng. Technol.* **2019**, *162*, 105726. [CrossRef]

11.   Tian, L.; Li, L. A Review on the Strengthening of Nanostructured Materials. *Int. J. Curr. Eng. Technol.* **2018**, *8*, 236–249. [CrossRef]

12.   Myers, A.; Kanvinde, A.; Deierlein, G.; Fell, B. Effect of weld details on the ductility of steel column baseplate connections. *Eng. Technol.* **2009**, *65*, 1366–1373. [CrossRef]

13.   Grilli, D.; Kanvinde, A. Embedded column base connections subjected to seismic loads: Strength model. *J. Constr. Steel Res.* **2017**, *129*, 240–249. [CrossRef]

14.   Torres, P.; Zareian, F.; Kanvinde, A. A hysteretic model for the rotational response of embedded column base connections. *Soil Dyn. Earthquake Eng.* **2018**, *115*, 55–65. [CrossRef]

15.   Falborski, T.; Hassan, A.; Kanvinde, A. Column base fixity in steel moment frames: Observations from instrumented buildings. *J. Constr. Steel Res.* **2020**, *168*, 1–13. [CrossRef]

16.   A36/A36M-19. *Standard Specification for Carbon Structural Steel*; Philadelphia American Society for Testing and Materials: Philadelphia, PA, USA, 2019.

17.   A193/A193M-17. *Standard Specification for Alloy-Steel and Stainless Steel Bolting for High Temperature or High Pressure Service and Other Special Purpose Applications*; American Society for Testing and Materials: Philadelphia, PA, USA, 2017.

18.   ACI Committee 318-14. *Building Code Requirements for Structural Concrete and Commentary*; ACI Committee: Farmington Hills, MI, USA, 2014.

19.   Ansys Inc. *ANSYS Multiphysics 16.0*; Ansys Inc.: Canonsburg, PA, USA, 2015.

20.   Gomez, I.; Kanvinde, A.; Smith, C.; Deierlein, G. *Shear Transfer in Exposed Column Base Plates*; Technical Report for American Institute of Steel Construction; American Institute of Steel Construction: Chicago, IL, USA, 2006.

21.   Ghassemieh, M. Evaluation of Stiffened End-Plate Moment Connection through Optimized Artificial Neural Network. *J. Software Eng. Appl.* **2012**, *5*, 156–167. [CrossRef]

22.   Bae, S.; Bayrak, O.; Jirsa, J.; Klingner, R. *Anchor Bolt Behavior in ASR/DEF-Damaged Drilled Shafts*; Technical Report N IAC 88-5DDIA004; Report for the Texas Department of Transportation, University of Texas at Austin: Austin, TX, USA, 2007.

23.   Desayi, P.; Krishnan, S. Equation for the stress-strain curve of concrete. *J. Am. Concr. Ins.* **1964**, *61*, 345–350.

24.   Gere, J.; Timoshenko, S. *Mechanics of Materials*, 3rd ed.; PWS-KENT Publishing Company: Boston, MA, USA, 1990.

25.   EN1993 Eurocode 3. *Design of Steel Structures*; Comité Européen de Normalisation (CEN): Brusels, Belgium, 2003.